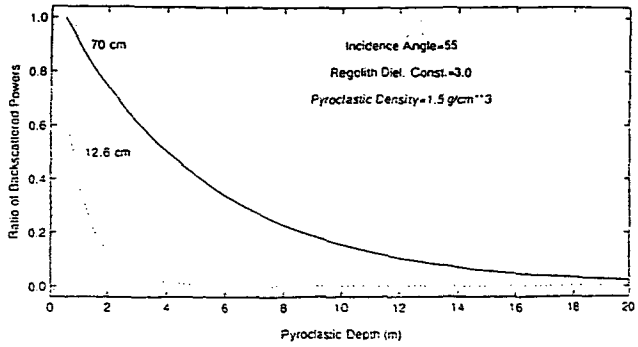

Fig. 1.

of pyroclastic deposits and analysis of 70-cm backscattering from the lunar regolith [8,9].

Input parameters to the model are the radar wavelength, the radar incidence angle, and the dielectric parameters of the pyroclastic layer and the regolith substrate. The model used here permits analysis of a pyroclastic layer with varying density as a function of depth. The electrical properties of an Apollo 17 glass sample [6] as a function of density ρ are used here:

$$\epsilon_r = 2.1^{\rho} \tan\delta = 0.0037\ \rho$$

where ϵ_r is the real dielectric constant and tan δ is the radar loss tangent. The real dielectric constant of the lunar regolith has been measured to be ~3.0, but may vary from mare to highland regions [10]. The incident circularly polarized wave is decomposed into horizontal and vertical polarized components, and the Fresnel transmission coefficients for each interface are calculated. Attenuation within the pyroclastic is assumed to be exp(-2αL), where L is the path length and α is the attenuation coefficient [11]

$$\alpha = k\,(0.5^{*}[(\tan\delta^2 + 1)^{0.5} - 1])^{0.5}$$

where k is the radar wavenumber in the pyroclastic deposit. This expression is solved numerically in our model for the varying density within the lossy medium.

All the scattered radiation within the regolith layer is assumed to be randomly polarized, with some total backscattering efficiency S. In our model, we thus combine the H- and V-polarized components within the regolith, multiply by S, and split the remaining power evenly between the two polarizations for the return trip to the surface. The energy that exits the pyroclastic is assumed to have random phase, but may have an elliptical polarization due to the differing H and V transmission coefficients. The scatter from an unmantled regolith is also calculated, and the two results are combined into a ratio of total mantled/unmantled backscatter. This cancels the S term in both expressions. The ellipticity of the final scattered wave is assumed to be close to unity. The results are plotted as a function of power ratio vs. depth for a given set of electrical and density parameters.

In mathematical terms, the H and V backscattered powers from a mantled region are

$$P_h = 0.25 * S * A^2 * (T_h^{s/p} * T_h^{p/r} + T_v^{s/p} * T_v^{p/r}) * T_h^{r/p} * T_h^{p/s}$$
$$P_v = 0.25 * S * A^2 * (T_h^{s/p} * T_h^{p/r} + T_v^{s/p} * T_v^{p/r}) * T_v^{r/p} * T_v^{p/s}$$

where A is the total attenuation factor, and the T terms refer to H- and V-polarized Fresnel transmission coefficients for the layer interfaces noted in their superscripts; s, p, and r refer to space, pyroclastic, and regolith respectively. The backscattered powers from an unmantled area are

$$Ph = 0.25 * S * (T_h^{s/r} + T_v^{s/r}) * T_h^{r/s}$$
$$Pv = 0.25 * S * (T_h^{s/r} + T_v^{s/r}) * T_v^{r/s}$$

Results: Figure 1 shows an example of this model for an incidence angle of 55°, corresponding to the Earth-based viewing geometry for the Aristarchus Plateau. The pyroclastic density was assumed to be a uniform 1.5 g/cm^3. The regolith real dielectric constant is assumed to be 3.0. Both 70-cm and 12.6-cm radar wavelengths are tested, and it is seen that the shorter wavelength is attenuated much more rapidly in the pyroclastic, as expected. The ratio between average 70-cm returns from the plateau and the mean lunar echo is ~0.30, implying a depth of 6–7 m based on these electrical parameters. This estimate is a lower bound; the actual buried highland terrain is likely much brighter than the Moon-wide average, implying a greater mantle depth.

Tests of the above model show that (1) it is relatively insensitive to variations in incidence angle between 20° and 60°, (2) it is insensitive to regolith dielectric variations from 2.5 to 4.0, (3) the scattered wave ellipticity is >85%, and (4) density variations with depth in the pyroclastic, within the narrow range permitted by realistic values of 1.5–2.0 g/cm^3, are not important unless the changes are very rapid. The value of the density at the upper surface of the layer is probably a satisfactory estimate for the overall density of such shallow deposits.

Conclusions: This technique may permit remote estimates of pyroclastic mantle depths from either Earth-based or lunar-orbital radar systems. A 3-km resolution map of the lunar nearside is available for 70-cm radar wavelength [12], and ongoing work at Arecibo Observatory provides additional data at 12.6-cm wavelength. We anticipate that such studies will be required in the planning stages of a lunar base project for resource assessment.

References: [1] Hawke B. R. et al. (1990) *Proc. LPS, Vol. 21*, 377–389. [2] Head J. W. (1974) *Proc. LSC 5th*, 207–222. [3] Wilson L. and Head J. W. (1981) *JGR*, 86, 2971–3001. [4] Gaddis L. R. et al. (1985) *Icarus*, 61, 461–489. [5] Lucey P. G. et al. (1986) *Proc. LPSC 16th*, in *JGR*, 91, D344–D354. [6] Bussey H. E. (1979) *Proc. LPSC 10th*, 2175–2182. [7] Zisk S. H. et al. (1977) *Moon*, 17, 59–99. [8] Moore H. J. et al. (1980) *USGS Prof. Paper 1046-B*. [9] Thompson T. W. and Zisk S. H. (1972) In *Prog. in Aero. and Astro.*, 83–117. [10] Hagfors T. and Evans J. V. (1968) In *Radar Astronomy*, 219–273. [11] Ulaby F. T. et al. (1986) In *Microwave Remote Sensing*, 67. [12] Thompson T. W. (1987) *Earth Moon Planets*, 37, 59–70.

A GROUND-BASED SEARCH FOR LUNAR RESOURCES USING HIGH-RESOLUTION IMAGING IN THE INFRARED.

C. R. Coombs and T. S. McKechnie, POD Associates, Inc., 2309 Renard Place SE, Suite 201, Albuquerque NM 87109, USA.

Introduction: When humans return to the Moon ("... this time to stay ...." [1]) lunar resources will play an important role in the successful deployment and maintenance of the lunar base. Previous studies have illustrated the abundance of resource materials available on the surface of the Moon, as well as their ready accessibility [e.g., 2–5]. Particularly worth considering are the lunar regional (2000–30,000 km^2) pyroclastic deposits scattered about the lunar nearside. These 30–50-m-thick deposits are composed

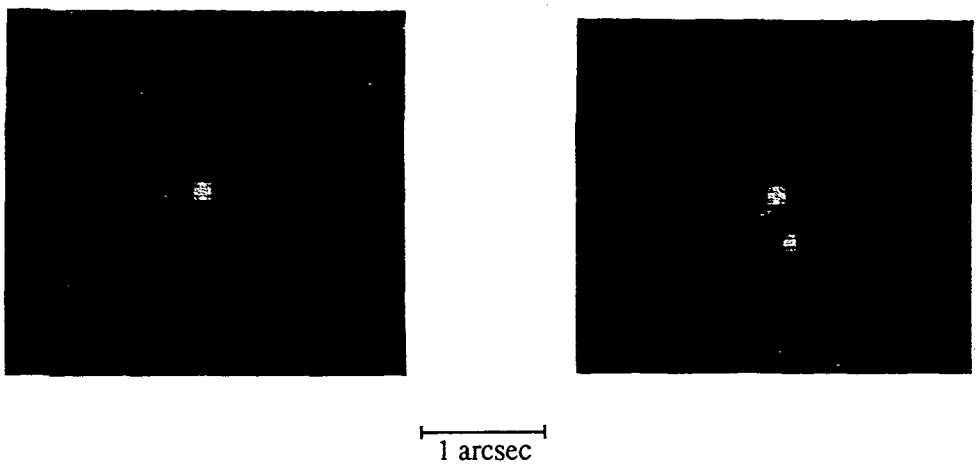

Fig. 1. Images of (a) Zeta Ophiuchi and (b) the 0.48-arcsec binary star Eta Ophiuchi obtained at 2.2 μm with the 4-m Kitt Peak telescope. The presence of the 0.1-arcsec cores easily allows resolution of the binary pair in spite of their close separation. Visual seeing was ~1–1.5 arcsec. Photos courtesy J. Christo (NOAO).

of fine-grained, unconsolidated titanium- and iron-rich mafic glasses and may be used as bulk feedstock for the beneficiation of oxygen, iron, titanium, sulfur, and other solar wind gases, or simply used as is for construction and shielding purposes. In this paper, we propose a groundbased observing survey of the resource-rich regions on the lunar nearside using a new imaging technique designed to obtain much higher resolution images, and more precise compositional analyses than previously obtainable.

High-Resolution Imaging: There is growing evidence that, contrary to popular wisdom, it should be possible to obtain diffraction-limited resolution at infrared wavelengths (>1 μm) from the ground without using adaptive optics. All that is needed is a telescope built to good enough optical specifications and the ability to compensate telescope motions. Left uncompensated, these motions, which are mainly caused by wind buffeting, can smear the image and cause serious loss of resolution. In this paper, an image stabilization system is proposed that will enable long-exposure imaging and spectroscopy to be carried out directly from the Earth with diffraction limited resolution.

According to recent atmospheric turbulence measurements [6–8], there is much less large-scale atmospheric turbulence than was previously thought. The lack of large structure implies much smaller RMS phase variation in the wavefronts entering the telescope. Over a 5-m aperture, the RMS wavefront height variation for 1-arcsec visible seeing is likely to be only about 0.3 μm, considerably smaller than previously thought. At visible wavelengths, these height variations will scramble the phases and give rise to badly degraded images. The phases of infrared wavelengths, however, are only partially modified by these same height variations so that only a portion of the light is scattered. Whereas this scattered portion will be imaged into a broad halo, the portion remaining intact, typically 50% of the light, will be focused into a diffraction limited core.

Figure 1 shows images of a single star and a 0.48-arcsec binary star obtained with the 4-m Kitt Peak telescope at 2.2 μm. The presence of the 0.1-arcsec core easily allows resolution of the binary. To obtain these images, a series of short exposures was taken to freeze the motion of the telescope. These were subsequently shifted and added so as to remove the motion. Long-exposure images identical to those shown can be obtained in real time by using an image motion compensation system such as shown in Fig. 2. Motion compensation can be carried out by first imaging a reference star on to the tracking detector array. The image stabilizer control drives the tip/tilt mirror so as to stabilize the core in the reference star image. Because of the very large isoplanatic angle associated with the core (several arcmin [7]) the arrangement simultaneously stabilizes the cores of all other objects, and hence enables diffraction-limited resolution over a very large angular region.

For extended objects such as the Moon, convenient reference stars (or point objects) for stabilizing the image may not be present. However, the presence of the core in the point spread function gives rise to abrupt intensity changes across edge images. By

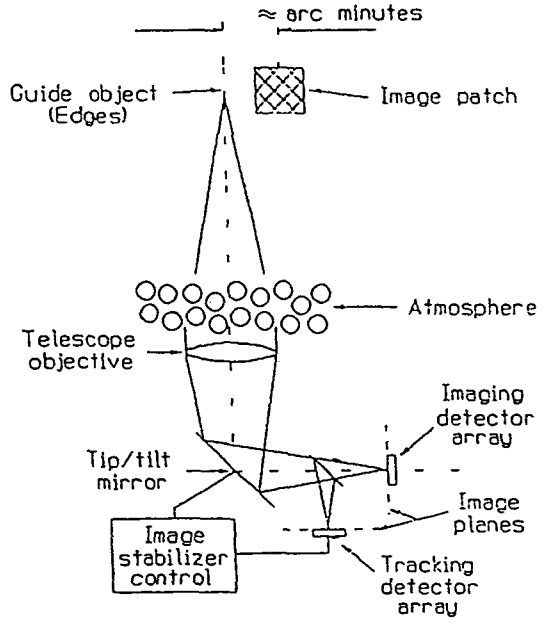

Fig. 2. Image stabilization using a tip/tilt mirror driven by a tracking detector and control electronics that lock on to cores or edges.

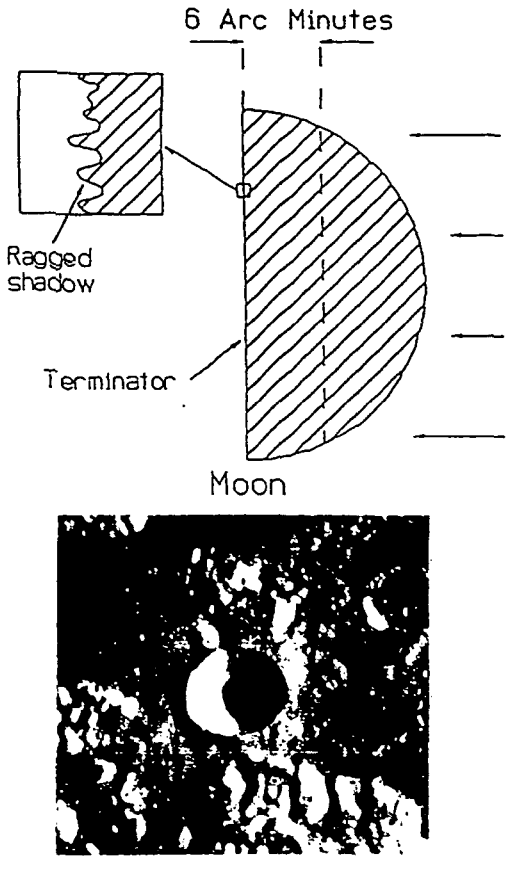

Fig. 3. The ragged edges at the lunar terminator provide suitable references for stabilizing the image. Using the configuration shown in Fig. 2 permits diffraction-limited imaging at IR wavelengths of a strip adjacent to the terminator several arcminutes wide.

tracking these abrupt intensity changes using two edges that are roughly at right angles to one another, image stabilization can be obtained to diffraction-limited accuracy. Suitable edges are found on the lunar terminator and at obliquely illuminated crater and basin edges (Fig. 3). Because the edges must lie within the isoplanatic angle of the region being imaged, it is only possible to image a strip a few arcminutes wide. Over the course of the lunar day (two weeks), however, a complete image of the lunar surface can be compiled using successive strips. With an infrared spectrometer mounted to this system, accurate compositional data will also be obtained.

The objective of this project is to conduct a lunar resource survey using image stabilization hardware of the sort shown in Fig. 2, in combination with a suitable edge-tracking algorithm. When the arrangement is used with existing 4–5-m class telescopes, 0.1-arcsec resolution (150 m) is expected at 2.2 μm. However, if the new 8-m (NOAO) telescopes are built to appropriate optical standards, diffraction-limited images should be obtained routinely at 1 μm. At this wavelength, 0.03-arcsec resolution is expected that, on the lunar surface, will result in imaging and spectroscopy being possible down to a 50-m spatial resolution element. With these resolutions, accurate geological and compositional maps may be constructed of the resource-rich regional pyroclastic deposits at a resolution currently not obtainable from Earth-based systems.

References: [1] President Bush, July 20, 1989. [2] Hawke B. R. et al. (1989) *Proc. LPSC 20th*, 249–258. [3] Mendell W. W., ed. (1985) *Lunar Bases and Space Activities of the 21st Century*, LPI, 866 pp. [4] Coombs C. R. (1988) Ph.D. dissertation, Univ. of Hawaii, 256 pp. [5] Blacic J. D. (1985) In *Lunar Bases and Space Activities of the 21st Century* (W. W. Mendell, ed.), 487–495. [6] T. S. McKechnie (1991) *J. Opt. Soc. Am.*, *8*, 346–365. [7] T. S. McKechnie (1991) *Proc. SPIE*, *1408*, 119–135. [8] C. E. Coulman et al. (1982) *Appl. Optics*, *27*, 155–160.

A REMOTE LASER MASS SPECTROMETER FOR LUNAR RESOURCE ASSESSMENT. R. J. De Young and M. D. Williams, NASA Langley Research Center, Hampton VA 23665-5225, USA.

The use of lasers as a source of excitation for surface mass spectroscopy has been investigated for some time [1]. Since the laser can be focused to a small spot with high intensity, it can vaporize and accelerate atoms of material. Using this phenomenon with a time-of-flight mass spectrometer allows a surface elemental mass analysis of a small region with each laser pulse. While the technique has been well developed for Earth applications, space applications are less developed. The Soviet Union attempted to use a pulsed Nd:YAG laser to analyze the surface of the Mars moon, Phobos, using an instrument called "LIMA-D" [2]. Laser-induced ions would have returned to spacecraft hovering 50 m above the Phobos surface. Unfortunately, the mission was unsuccessful for reasons unrelated to the instrument.

NASA Langley recently began a research program to investigate the use of a laser to create ions from the lunar surface and to analyze the ions at an orbiting spacecraft. A multijoule, Q-switched Nd:YAG laser would be focused to a small spot on the lunar surface, creating a dense plasma. This plasma would eject high-energy ions, as well as neutrals, electrons, and photons, as shown in Fig. 1. Such a system is shown in schematic form in Fig. 2. Here the spacecraft is 10 km above the lunar surface, and for the parameters shown, would detect 10^7 ions per laser shot. The travel time and velocity of the elemental ions created is shown in Fig. 3, assuming a 10-eV equilibrium plasma. Detection of ions at large distance requires that the flight path be a larger than the collision mean-free path as shown in Fig. 4 where the mean-free path (km) is shown for various regions of space. The lunar environment provides very long collision mean-free paths for the detection of laser-produced ions.

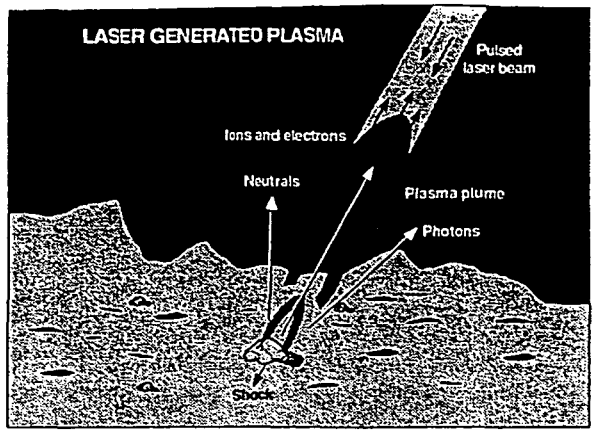

Fig. 1.